Chain-Length Dependence of the Dissociation Dynamics of Oriented Molecular Adsorbates: *n*-Alkyl Bromides on GaAs(110)

Khalid A. Khan, Nicholas Camillone III,* and Richard M. Osgood, Jr.

Columbia Radiation Laboratory, Columbia University, New York, New York 10027

Received: March 5, 1999; In Final Form: April 30, 1999

Brominated hydrocarbons adsorbed on semiconductor surfaces serve as ideal model systems for investigating the photoinduced chemistry of oriented molecules in the condensed phase. Under UV irradiation these adsorbates dissociate via attachment of photoexcited substrate electrons giving rise to energetic alkyl and surface-bound bromine fragments. In this report we describe the effect on the fragmentation dynamics due to systematic variation of the complexity (alkyl chain length) of the adsorbate. Increasing the length of the alkyl chain leads to distinct changes in the alkyl fragment angular distributions. For methyl bromide, the angular distribution is dominated by a focused beam of directly ejected hyperthermal methyl radicals at 44° (in the [0$\bar{1}$] direction) from the surface normal. While a similar direct beam is observed for ethyl and propyl bromide, inelastic scattering of these fragments is found to result in increased importance of a slower diffuse $\cos^n \theta$ desorption. In addition, significant retention of alkyl fragments is detected by postirradiation thermal desorption measurements for these longer-chain homologues. Increasing the number of degrees of freedom of the adsorbate is also observed to dramatically alter the energetics of the ejection of the photofragments from the surface. As the number of carbons in the fragment is increased from one to three, the average energy of the directly ejected radicals decreases from 1.48 to 1.1 to 0.69 eV (UV incident at $\lambda = 193$ nm). Variations in the energy and angular distributions are discussed in terms of initial adsorbate orientation, energy partitioning into rovibrational modes, and influence of radical−surface interactions.

1. Introduction

Photoinduced substrate−adsorbate electron transfer resulting in dissociative electron attachment has been shown to be an important mechanism in the photoinduced chemistry of molecules adsorbed on clean metal and semiconductor surfaces.[1−6] In sharp contrast to dissociation by direct photon absorption by the molecules (i.e., direct photolysis, a process which is strongly quenched on these high-dielectric substrates at monolayer coverages), this particular substrate-mediated process has been shown to proceed with relatively high efficiency.

Previous studies of electron attachment have centered on two broad issues: the detailed physics of the attachment process and the dynamics of the fragmentation process. There exists an extensive body of literature which examines the attachment process both theoretically and experimentally for both gas-phase and adsorbed species. The most detailed studies of the adsorbed state have utilized monochromatized electrons from external electron-beam sources.[7,8] These studies have shown that the cross sections for dissociative electron attachment of molecules such as the alkyl halides are exceedingly sensitive to the surrounding molecular environment. For example, the presence of noble gas spacer layers has been shown to increase dissociative yields by several orders of magnitude (relative to the gas phase) via charge-induced dipole stabilization of the anionic state.[8]

Related effects have recently been observed for the case of photoinitiated electron transfer from metal and semiconductor substrates to molecular adsorbates. These studies, which employ UV and visible irradiation to photoexcite substrate electrons, have provided a unique window into the electron dynamics of charge transfer both above *and below* the substrate vacuum level.[6,9] While observations have been made for a variety of adsorbed species, one of the most consistently explored classes has been the normal alkyl halides. This class of molecules serves as a model system for understanding substrate-mediated dissociative electron attachment. Measurements of electron attachment to alkyl halides at monolayer coverages have shown low photon-energy thresholds compared to those found for dissociation via direct photolysis in the gas phase, a result consistent with substrate mediation and strong image−charge interaction lowering of the anionic state on high-dielectric surfaces.[9] In addition, strong adsorbate−substrate coupling can act to decrease anion lifetimes via quenching,[10] resulting in a decrease of the dissociative electron attachment cross section compared to that found in the gas phase.[6]

Less work has been reported on the dynamics of the fragmentation process following dissociation by electron attachment. These measurements have shown that fragmentation of the adsorbate typically results in the ejection of a hydrocarbon radical and, in some cases, halogen anions.[11] An understanding of the dynamics of the ejected fragments has been shown to provide valuable insight into the features of the photon-driven surface chemistry. For example, dynamical measurements of fragment translational energies have been an essential element in distinguishing between bond cleavage by electron attachment and direct photolysis, since the energetics of the latter process agree well with those observed in gas-phase photodissociation measurements, while those of the former do not.[4,12,13] Dynamical measurements of electron attachment on semiconductor and metal surfaces have also revealed a weak dependence of fragment kinetic energies upon the incident photon energy.[3,4,14] In addition, ejected fragment angular distributions have been

10.1021/jp990782m CCC: $18.00
Published on Web 06/11/1999

directly correlated with preirradiation orientation of the adsorbed molecules.[4,15,16]

Our primary efforts have been the experimental examination of substrate-mediated photoinduced fragmentation on highly corrugated semiconductor surfaces. Our experiments have focused on a series of methyl halides and examined fragmentation resulting from excitation at visible and UV wavelengths. Study of these systems has provided insight into the dynamics of the interactions between reactive radical and ionic species and surfaces. For example, for methyl halides (CH_3Cl, CH_3Br, and CH_3I) adsorbed on GaAs(110), time-of-flight (TOF) techniques have been employed to probe the energetics of the desorbing methyl radicals.[4,14] Depending on the methyl halide, the average kinetic energy of the methyl fragment ranged from 0.6 to 1.5 eV, comparable to the energies found for dissociation on metal surfaces.[4] Interestingly, distinct fragment angular distributions indicated a preferred desorption direction of the methyl fragment. For all three methyl halides, the methyl fragment flux was found to peak at ~45° from the surface normal in the $[0\bar{1}]$ direction of the GaAs(110) surface.[14] Subsequent NEXAFS measurements[16] and ab initio calculations[15] on these systems confirmed that the sharp peak in the TOF angular distributions reflected the initial orientation of the molecule, which is determined, to a large extent, by strong molecule-dipole−surface-dipole interactions. These observations suggest that a large fraction of the methyl fragments are not significantly scattered as they exit the near-surface region after cleavage of the C−Br bond. In contrast, scattering *has* been reported for direct photolysis of methyl halides on insulator surfaces, due to the antiparallel alignment on these surfaces.[17,18]

These results raise the question of how the adsorbate fragmentation dynamics change as the complexity of the molecule increases. It is known that the yield and the chemistry of substrate-mediated dissociative electron attachment depend significantly on molecular size. This dependence has been examined, for example, for a series of halogenated methanes.[11,19] Similarly, for the normal alkyl bromides, the length of the hydrocarbon chain has also been shown to affect yield and chemistry.[6] A detailed systematic series of measurements would thus be useful to examine how fragment dynamics change with molecular length and complexity. Clearly, fragment mass, internal degrees of freedom, and relative molecular orientation should all have important effects on the dynamics. In this regard, recent measurements of the dissociation of ethyl bromide on GaAs(110) revealed differences in the dynamics of the ethyl compared to those of the shorter methyl fragments. The changes in the dynamics due to the presence of an additional CH_2 group were manifested in differences in the velocity and angular distributions of the ejected fragments. Furthermore, postirradiation TPD studies revealed that some fraction of ethyl fragments remained trapped at the surface, the result of a dynamical channel previously unobserved in the methyl halides.[5]

This paper presents a systematic measurement of the similarities and differences in the photofragment dynamics as the length of the alkyl bromide is increased over the homologous series: methyl, ethyl, and propyl bromide. Since dissociation of all three molecules occurs by way of C−Br bond cleavage, the experiments systematically study the dependence of the fragment ejection dynamics upon the mass and complexity of the species desorbing from the highly corrugated GaAs(110) surface. Furthermore, by changing the wavelength of the dissociating light, the energy transferred to the adsorbate−substrate complex can be varied. Thus, the effect of the fragment energy on the dynamics can also be probed.

2. Experimental Section

The details of the experimental setup are similar to those described in our previous work.[5,12,14,20] All experiments were performed in a UHV system with a two-tier chamber with a typical base pressure of 2×10^{-10} Torr. A gate valve separates the two levels. The top part of the chamber was equipped with a quadrupole mass spectrometer (QMS) and an effusive-beam gas doser. A low energy electron diffraction (LEED) apparatus for measurement of crystal order and orientation and an ion gun used for sputter cleaning the sample surface were housed in the lower part of the system. The lower chamber was used exclusively for crystal preparation. Temperature-programmed desorption measurements (TPD) and angle-resolved TOF measurements were made in the top chamber. A single-crystal sample (obtained from Atramet) of GaAs(110) measuring $1 \times 1 \times 0.1$ cm with *n*-type ($1.4 \times 10^{17}/cm^3$) Si doping was mounted on a 0.125-mm-thick strip of Mo foil in good thermal contact with the bottom of a liquid-nitrogen reservoir. A crystal manipulator allowed for (*z*-axis) translation of the sample assembly between the two chambers. The manipulator also rotated the crystal about an axis (the *z*-axis) which runs through the center of the crystal and translated it in directions perpendicular to this axis. The crystal was mounted such that the $\langle 1\bar{1}0 \rangle$ direction is parallel to the axis of rotation. It was heated resistively by passing a current through the Mo foil. The temperature was measured by a thermocouple spot welded to the foil near the middle of the crystal.

Repeated cycles of sputtering with 500 eV Ar^+ ions at 300 K and subsequent annealing to 840 K were used to prepare the GaAs crystal. After surface preparation, a sharp (1×1) LEED pattern was observed. The quality of the crystal surface was further ascertained by measuring a series of CH_3Br desorption spectra. Previous experiments have established the shape of these TPD curves for surfaces relatively free of defects.[20] The determination of the [01] and $[0\bar{1}]$ directions was accomplished through the use of the dynamic LEED procedure described in ref 21.

Methyl bromide (99.5+%, Aldrich), ethyl bromide (99+%, Aldrich), and propyl bromide (99%, Aldrich) were the three alkyl bromides used in this study. The latter two were further purified by several freeze−pump−thaw cycles. Molecules were deposited on a clean crystal surface by exposing the crystal, cooled to 90 K, to controlled amounts of these gases through a pinhole doser. Monolayers were prepared by first growing a multilayer of the desired compound and then desorbing the excess amount by annealing at a temperature just below the onset of desorption of the monolayer. Thermal reactions between the adsorbate and GaAs both before and after exposure to UV light were studied with mass-resolved TPD. All TPD spectra were recorded over the 90−840 K temperature range with a computer-controlled ramp rate of 2.5 K/s with the crystal positioned such that the QMS line-of-sight and surface normal were parallel (i.e., $\theta = 0°$, detection angles referenced with respect to the surface normal).

For the TOF measurements, monolayers were exposed to the unpolarized UV light output from an excimer laser with 20-ns pulses at 20 Hz with wavelengths of 193 nm (ArF), 248 nm (KrF), or 351 nm (XeF). The laser beam was introduced through either of two fused silica windows on the top chamber such that its angle of incidence on the surface was 60° with respect to the line-of-sight of the QMS. The laser fluence in these experiments varied from 0.5 to 1 mJ/cm^2 per pulse. The power was measured before and after each run with a calibrated thermopile detector (Scientech 381UV) placed in front of the

laser entrance port. Operation of the laser at low power prevented any significant surface heating, thereby eliminating laser-induced thermal desorption of the adsorbate. The total number of photons absorbed by the adsorbate-covered surface was calculated using the wavelength- and angle-dependent reflectivity of the substrate according to Fresnel's equations[22] and tabulated indices of refraction for GaAs.[23]

TOF spectra for different detection angles were recorded by rotating the sample manipulator about the *z*-axis. All TOF spectra were normalized to take into account the absorbed photon density and the variation in the area illuminated and subtended by the detector as the sample is rotated. The TOF spectra were fit to modified Maxwell−Boltzmann distributions in order to extract quantitative information (i.e., average kinetic energy) on the photofragment dynamics. The details of this fitting procedure have been discussed in ref 5.

3. Results

Our group previously has shown that monolayers of alkyl bromides (methyl, ethyl, and propyl bromide) on GaAs undergo C−Br bond cleavage on exposure to UV light.[4−6] Therefore, in the first section below, we briefly present the highlights from this earlier work that are relevant to the current investigation. We begin by summarizing the adsorption/desorption characteristics of the different monolayers on GaAs as determined by TPD spectroscopy. The substrate-mediated photochemistry of the adsorbate−substrate complex on exposure to UV light is also discussed. The primary focus of this paper will be on the fragment dynamics following dissociation. A detailed discussion of the chain-length dependence of the electron-transfer process and presentation of related experimental results are the subjects of a separate publication.[6]

3.1. Thermal Desorption and UV-Initiated Chemistry of *n*-Alkyl Bromide Monolayers. The nature of the adsorbate−substrate system was characterized carefully before exposure to UV light. TPD spectroscopy has been used to extensively study the adsorption of methyl, ethyl, and propyl bromide on GaAs(110) at liquid-nitrogen (90 K) temperatures. TPD results were used to ascertain the chemical reactivity of these molecules with GaAs, the binding energies with the surface, and the nature of the adsorption kinetics. For details, the reader is referred to the following: refs 4−6 and 20.

The alkyl bromides studied here have been shown by our group to adsorb molecularly on GaAs(110) at 90 K.[4−6] Mass-resolved TPD results show no evidence of molecular dissociation after ramping a 1 ML adsorbate-covered surface to 840 K. The desorption curves for the alkyl fragment for each of the adsorbates are shown in Figure 1. This figure also shows the desorption energies for monolayers of the three adsorbates calculated using the Redhead method.[24] The desorption energy of the alkyl bromides on GaAs increases with the number of carbon atoms. The 0.05 eV per CH_2-group increase in the desorption energy is consistent with an expected increase in the van der Waals interaction energy based on simple Lennard−Jones potentials.[6]

To ascertain the effects of UV (λ = 193, 248, and 351 nm) light on monolayers of the alkyl bromides, TPD results from an adsorbate-covered surface which was exposed to photons were compared with those from an identically-prepared unexposed surface. The integrated area of the molecular desorption peak in the postirradiation TPD spectrum was less than that in the spectrum obtained for the unirradiated monolayer. This difference resulted from loss of the molecular adsorbate on exposure to UV light. In concert with this loss, mass-resolved

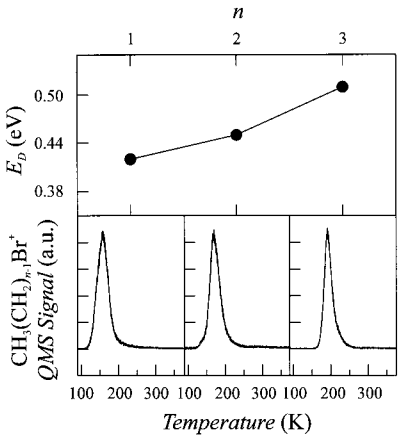

Figure 1. Top panel shows the desorption energy, E_D, for the three molecules. The lower three panels show temperature-programmed desorption spectra for methyl bromide (n = 1), ethyl bromide (n = 2), and propyl bromide (n = 3) at 1 ML coverage.

TPD spectra of the UV-treated monolayers identified surface-bound hydrocarbon fragments and gallium bromide. The only hydrocarbon fragments observed were ethyl radicals and ethene for ethyl bromide and propyl radicals and propene for propyl bromide. No hydrocarbon species were retained on the surface for irradiated monolayers of methyl bromide.

These observations have been shown to be due to UV light-induced C−Br bond cleavage yielding alkyl fragments and bromine species as summarized by the chemical equation:[4−6,20]

$$\mathrm{RBr(ad)} + \mathrm{e_{VB}^-} \xrightarrow{h\nu} \cdot\mathrm{R(g,ad)} + \mathrm{Br^-(ad)} \qquad (1)$$

where e_{VB}^- is an electron excited from the valence band and Br^-(ad) is bromine that subsequently reacted with the surface gallium. The ethene and propene were shown to be products of β-hydride elimination of the respective alkyl fragments trapped on the surface.[5,6] Due to the identical desorption temperature (∼616 K) of the radical and its corresponding alkene, we were unable to determine by TPD whether the elimination reaction is initiated during or prior to heating of the surface.[5]

Whereas these TPD measurements show that the alkyl bromides undergo bond scission and that some of the dissociation products are trapped on the surface, TOF measurements reveal that some of the alkyl fragments are ejected from the surface. For methyl, ethyl, and propyl bromide we observe ejection of only methyl, ethyl, and propyl radicals, respectively, upon exposure to UV light. The following sections present our TOF results in detail.

3.2. Photofragment Dynamics. Energy and angle-resolved TOF measurements were made on all three systems to study the dynamics of the photofragments at 1 ML. The UV-induced C−Br bond cleavage in the three adsorbed species resulted in the ejection of energetic alkyl radicals from the surface over a wide range of angles detected in the plane defined by the surface normal and the [01] surface vector. As detailed below, our results show that both the fragment angular distribution and energetics are strongly chain-length-dependent.

3.2.1. Angular Distribution Measurements. Figure 2 shows the angular distributions that resulted from exposing monolayers of the three adsorbed species to 193-nm light. The figure displays the total integrated flux (circles) of the alkyl fragments as a function of the detection angle. Although the fragments are observed over a wide range of angles for all these alkyl bromides, it is clear from the distributions that there is a relatively narrow lobe peaked in the [0$\bar{1}$] direction. In addition

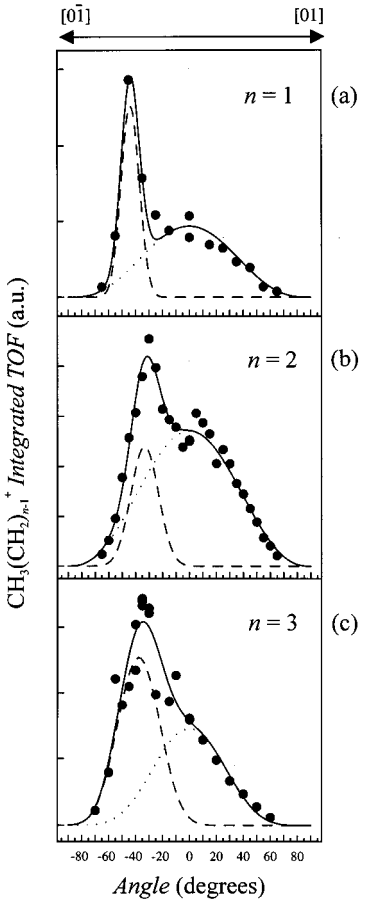

Figure 2. TOF angular distributions for the three alkyl fragments after exposure of 1 ML of the molecular adsorbate to 193-nm light. The solid line through the data points is the sum of the slow (dotted line) and fast (dashed line) components from the fit of the function $f(\theta)$ described in the text.

to this feature, the distributions all exhibit a broad component which extends to positive detection angles. These qualitative similarities in the angular distributions for the three molecules are, with some important changes, also observed when the adsorbate dissociation is initiated with 248- and 351-nm light.

Latent in these angular distributions is important information on the energetics of the alkyl fragments. For example, in a *previous* study we showed that the angular distribution from the ethyl bromide-covered surface is the sum of *two energetically* distinct ethyl fragment channels.[5] TOF spectra of ethyl radicals made at positive detection angles could be described with a single modified Maxwell−Boltzmann (MMB) distribution with an average energy of 0.6 eV.[25] In contrast, the TOF spectra taken at negative observation angles could be accurately described by the sum of this 0.6 eV channel and by an additional higher-energy, ∼1 eV, MMB distribution.

In fact, analysis of this earlier ethyl bromide TOF data revealed[5] that the angular distribution could be described by the following expression:

$$f(\theta) = A_S \cos^m \theta + A_F \cos^q(\theta - \theta_p) \qquad (2)$$

It is possible to uniquely ascertain the contribution of the slow channel to the total angular distribution by first fitting eq 2 to the integrated TOF area for positive observation angles only, with $\cos^q(\theta - \theta_p) = 0$. Using A_S and m from this fitting step, the relative contribution of the two channels to the total desorbate flux distribution is then obtained by fitting the total

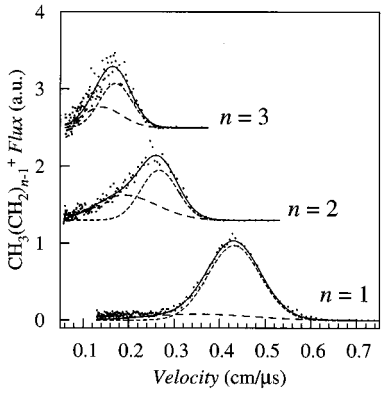

Figure 3. Flux-weighted velocity distributions for the three alkyl fragments. The solid line is a fit of the sum of two modified Maxwell−Boltzman distributions, a fast component and a slow component.

distribution to eq 2. Therefore, the first term in eq 2 isolates the isotropic component of the slow ethyl fragments ($m = 2.5$) from the total angular distribution, while the second term accounts for the fast-channel ethyl fragments with $q = 31$ and $\theta_p = -33°$. The sum of the two terms, $f(\theta)$, as shown in Figure 2b, accurately fits the angular distribution for ethyl fragments.

Given the qualitative similarities in the angular distributions for methyl and propyl fragments with that of ethyl fragments (see Figure 2), it is reasonable to expect that these species would also exhibit bimodal velocity distributions. In fact, fits based on isolation of the slow-channel MMB component at positive observation angles show that the observed velocity distributions for methyl and propyl fragments at negative detection angles, like those for ethyl fragments, are well-described by the sum of two MMB distributions. We, therefore, can fit the total angular distributions for methyl and propyl fragments to eq 2 and interpret the two components that simulate the angular distribution as two distinct energetic alkyl fragment channels. The methyl and propyl fragments in the slow channel were found to have an average energy of 1.1 and 0.5 eV, respectively. Furthermore, the total integrated methyl and propyl TOF signals at positive detection angles are well-described by $\cos^m \theta$ with $m = 2.7$ and 4.6, respectively. Compared to the slow isotropic methyl and ethyl ejection channels, the slow-channel propyl fragments leave the surface with an angular distribution that is more tightly focused about the surface normal.

Figure 2c reveals that a substantial part of the total angular distribution of the propyl desorbate flux is focused into a relatively sharp feature peaked at −38°. As in the case of the ethyl fragment distribution, this feature describes the more energetic MMB distribution (average energy ∼ 0.70 eV). Both this and the slower-channel distribution (average energy 0.50 eV) are needed to describe fully the propyl fragment velocity distributions measured at negative detection angles (see Figure 3). Similarly, the angular distribution of the methyl fragments has a significant component peaked at −44° describing the faster (average energy ∼ 1.5 eV) desorbing fragments in addition to a small, slower, isotropic component. Although the former feature of the angular distribution has been observed and studied extensively in the past,[4,6,14,16] the latter cosine-like component was masked by the presence of a surface-defect-sensitive feature[14,26] which was not observed in this current study.

We have established that it is possible to separate the angular distributions for the fragments in terms of contributions from *slow* and *fast* alkyl radicals ejected from the surface. While our measurements reveal a qualitative similarity among the angular distributions (see Figure 2), as Table 1 shows, quantitative

TABLE 1: Photofragment Angular Distribution Parameters[a]

n	θ_{peak} (deg)	ΔW_f	m	ΔW_s (deg)
1	−44	16	2.7	78
2	−33	24	2.5	82
3	−38	37	4.6	61

[a] Here, n is the number of carbons in the molecule, θ_{peak} is the position of the peak, ΔW_f is the width of the direct (anisotropic) lobe, m is the exponent describing the indirect (isotropic) lobe (see eq 2), and ΔW_s is the width of the indirect lobe.

analysis reveals that the characteristics of the angular distributions associated with the two desorption channels change considerably when the alkyl chain length is varied. It would be reasonable for these changes to be closely related to the detailed energetics involved in the dissociation process, and in fact, it will be argued below that the measured decrease in the kinetic energy of the alkyl desorbate with an increase in the chain length can reasonably account for the differences observed in the angular distributions.

3.2.2. Comparison of the Velocity Distributions. For fragments created at 193 nm and detected at −45°, the average kinetic energy of the ethyl and propyl fragments has been measured, respectively, to be approximately 35% and 50% less than the average kinetic energy of the methyl fragments. Figure 3 shows the velocity profiles recorded for the three alkyl radicals at −45° when dissociation of the adsorbates is initiated with 193-nm light. The solid line in each of the spectra is a sum of two MMB distributions. Contributions of the separate MMB distributions describing the slow and fast channels at this angle are also illustrated. The strong dependence of the velocity distributions for both channels on the chain length of the desorbing species is clearly evident in this figure.

The average energy associated with the two desorbing channels is plotted as a function of the number of carbon atoms in Figure 4. The average kinetic energy of the *fast channel* (closed circles) decreases by 0.4 eV per CH_2 group. Although quantitatively different, a similar trend in the average kinetic energy of the slow channel (open circles) with increased chain length is also observed. In the Discussion section we will argue that this decrease in the kinetic energy with increasing chain length appears not to be due to an increase of the mass of the fragment with increasing chain length; instead we must consider the important role that partitioning of energy into rovibrational degrees of freedom of the fragment plays in the dissociation dynamics.

3.2.3. Wavelength-Dependence Measurements. One useful approach for examining the photoinduced desorption dynamics of fragments from a surface is to examine the variation of this response with the photon energy. Several groups have observed fragments produced by photoinduced substrate-electron-mediated dissociation of adsorbates to exhibit little or no dependence on the photon energy.[27,28] As we will show, more significant effects are seen for the molecular series examined here.

Previous measurements on methyl bromide have shown that both the energy and angular distributions are nearly invariant with the wavelength of the incident radiation.[4,14] Figure 5 shows, for example, that changing the dissociating wavelength from 193 to 351 nm, a decrease of ∼3 eV, results in only a 14% decrease in the average kinetic energy of the methyl fragments detected at −40°.

It is clear from the angular distributions presented in Figure 2 that their anisotropies can be characterized by the ratio of the intensities of the narrow distribution, peaked at ∼ −40°, to the broad angular distribution centered at 0°. This ratio can be accurately calibrated using the fitting procedure described in section 3.2.1. Alternatively, a simpler but equally valid characterization of the anisotropy of the angular distributions can be obtained by introducing a parameter R defined by

$$R \equiv \frac{I_{TOF}^{-40}}{I_{TOF}^{0}} \tag{3}$$

where I_{TOF}^{θ} is the total TOF signal at detection angle θ. R serves as a simple, phenomenological parameter that characterizes the bimodality of the angular distribution. (Note: for purposes of comparison of the degree of change of the bimodality with wavelength, the ratios, R in Figure 5, for each of the three fragments have been normalized to their values at $E_\gamma = 6.4$ eV.) Notably, for methyl bromide (see Figure 5), R is independent of the excitation wavelength, within our experimental uncertainty. This constant value for R indicates that the angular distribution is independent of the dissociating wavelength. Results from such a characterization of the angular distributions are in agreement with previous angle-resolved measurements of the methyl fragments from the dissociation of methyl bromide adsorbed on GaAs(110) with 193-, 248-, and 351-nm light.[4]

However, in the general case, we find that the angular distribution for the photofragments is not strictly independent of the wavelength of the light used to dissociate the molecular adsorbate. In fact, for the cases of ethyl and propyl bromide

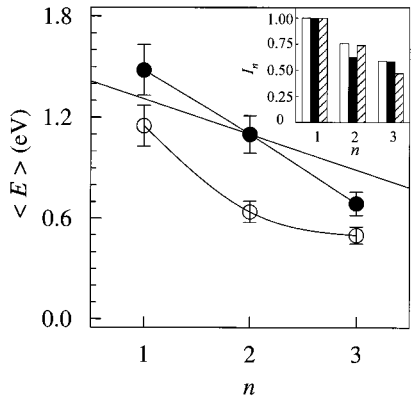

Figure 4. Average kinetic energy of the slow (open circles) and fast (closed circles) alkyl fragments at 193 nm. Results from the calculation following eq 6 in the text are represented by the downward sloping line passing through the data at $n = 2$. Inset shows histogram of the fraction of the available energy partitioned into translational energy of the alkyl fragment, $CH_3(CH_2)_{n-1}$, following UV dissociation for alkyl iodides (white) in the gas phase, alkyl chlorides (black) in the gas phase, and alkyl bromides (hatched) physisorbed on GaAs(110).

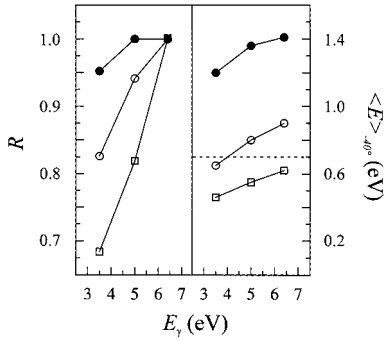

Figure 5. Left panel shows the anisotropy of the angular distributions, R, as a function of incident photon energy, E_γ. Right panel depicts the measured average kinetic energy of the fragments at −40°. Solid circles, methyl bromide; open circles, ethyl bromide; open squares, propyl bromide.

we have observed a correlation between the energetics of the alkyl fragments and the bimodality or anisotropy of their angular distributions. For example, Figure 5 shows that as the dissociating wavelength is increased from 193 to 351 nm, the average kinetic energy of ethyl and propyl fragments ($\theta = -40°$) decreases by 28% and 26%, respectively. This decrease in the fragment energy is also accompanied by a decrease in *R*. This experimentally observed correlation between *R* and the average fragment kinetic energy for both ethyl and propyl photofragments suggests that fragment energetics are important for the understanding and interpretation of angular distributions.

The velocity and angular distributions of the ethyl and propyl fragments exhibit qualitatively similar wavelength dependencies. However there are a number of quantitative differences in the dynamics. First, the ~30% decrease observed in the average kinetic energy for both fragments upon decreasing the incident photon energy from 6.4 to 3.5 eV is accompanied by a much larger decrease in the angular anisotropy, *R*, in the case of the propyl fragment than in the case of the ethyl fragment (see Figure 5). We find that *R* is 35% smaller at 351 than at 193 nm for the propyl fragment, whereas for ethyl fragments, only an 18% difference is observed in *R* between these two wavelengths. Furthermore, the change in *R* for the ethyl fragments at 248 and 193 nm is relatively insignificant (~6%, within our experimental uncertainty). The nearly identical values of *R* for ethyl bromide at 193 and 248 nm are consistent with our earlier study which decomposed the angular distributions and determined that the ratio of the two components remained the same when the wavelength was changed from 193 to 248 nm (see ref 5). However, this insignificant change in *R* for the ethyl fragments between these two wavelengths is in sharp contrast to the much larger decrease of 20% in *R* for the propyl fragments for an identical change in the average kinetic energy of the two fragments.

As stated above, for a given excitation photon energy, the average kinetic energy, $\langle E \rangle$, of ethyl fragments is larger than that for the propyl fragments. For example, ethyl fragments have a substantially larger $\langle E \rangle$ of 0.90 eV at 193 nm compared with 0.62 eV for the propyl fragments. When the wavelength of the incident radiation is increased to 248 nm, the $\langle E \rangle$ of both the ethyl and propyl fragments decreases by ~0.1 eV to 0.8 and 0.5 eV, respectively. This drop in $\langle E \rangle$ for the ethyl fragments results in a very small (6%) decrease in *R*, while the same drop for propyl results in a very large (~18%) decrease in *R*. Interestingly, as the wavelength is further increased to 351 nm and the $\langle E \rangle$ of both ethyl and propyl fragments drops by another ~0.1 eV, both fragment distributions exhibit relatively large decreases in *R*. At 351 nm the $\langle E \rangle$ of the ethyl fragments has dropped to less than 0.7 eV. These results establish the correlation, dramatically illustrated by Figure 5, that *R* is strongly effected only when the $\langle E \rangle$ of the fragments drops below ~0.7 eV. This correlation suggests that in order for the angular distribution to vary significantly with wavelength, the average kinetic energy of the photofragments (both ethyl and propyl species) has to be below an energetic threshold. The invariance of the methyl angular distributions with wavelength is consistent with the presence of such an energetic threshold, since the average energy of these fragments is significantly above 0.7 eV. We believe that this threshold is related to an energetic threshold to desorption. These ideas will be explored in further detail in the Discussion section below.

The average energy of fragments detected in the slow channel ($\theta = 0°$) does not necessarily decrease with a decrease in the photon energy. In fact for propyl fragments (see Figure 6, open squares) the average kinetic energy at the three photon energies is approximately constant given our experimental uncertainty. Also note that at 351 nm the average velocity of the propyl fragments at both detection angles ($\theta = 0°$ and $-40°$) is equal to 0.46 eV. Furthermore, the average energy for the slow-channel ethyl fragments at this wavelength also has, within experimental uncertainty, this same value (0.43 eV). The only significant change in the average energy of the desorbing species in the slow channel is observed for the ethyl fragments when the wavelength is decreased from 351 to either 193 or 248 nm. At the latter two wavelengths the average energy is ~0.65 eV, much larger than the 0.43 eV at 351 nm. These observed trends in the energetics have implications for the fragment dynamics which will be discussed in greater detail below.

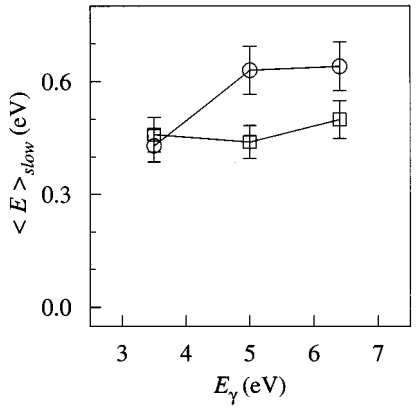

Figure 6. Average kinetic energy associated with the slow channel for ethyl fragments (open circles) and propyl fragments (open squares) for the different incident photon energy, E_γ.

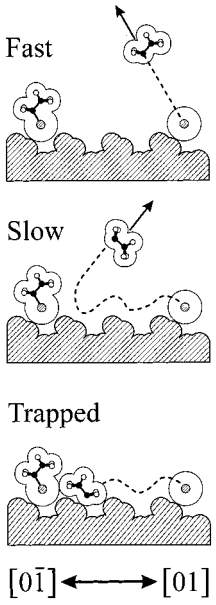

Figure 7. Schematic representation of the three observed energetic channels for the desorption of ethyl fragments. The shaded region represents the (110) terminated reconstruction of GaAs.

3.2.4. The Three Energetic Photofragment Channels. The results from our TPD and TOF angular distribution measurements presented above establish three energetically distinct photoreaction channels (see Figure 7): (1) the fast channel is observed to be strongly peaked at negative detection angles, (2) the slow channel is isotropic, peaked at the surface normal, and (3) the trapped channel is comprised of fragments fully accommodated on the surface. The origin of these different

channels remains to be established. In this section we will argue that all three energetic channels are different dynamical manifestations of the same dissociation event.

The fast channel observed in the TOF from *methyl* and *ethyl* bromide-covered surfaces has been shown to be the result of fragments ejected from the surface during an electron-mediated impulsive force from the C−Br bond rupture.[5,14] In fact, previous studies[5,14,16] have interpreted the anisotropic angular distributions produced by methyl and ethyl fragments to be indicative of the orientation of the adsorbate molecule on the corrugated semiconductor surface, prior to excitation of the adsorbate. The sharp feature peaked at −44° in the angular distribution (see Figure 2a) has been interpreted as reflecting the angle between the C−Br bond and the surface normal.[4,14] Strong agreement with results from both NEXAFS measurements[16] as well as ab initio cluster calculations[15] supports this interpretation. More recently, studies involving similar measurements with ethyl bromide as the adsorbate suggested that the peak at −33° in the angular distribution also reflected a tilted orientation, toward the [0$\bar{1}$] direction, of the adsorbed ethyl bromide molecule.[5] Due to the more complicated fragment dynamics in this system, it was difficult to ascertain as accurately the angle between the C−Br bond and the surface normal as for CH_3Br. Nevertheless, the high energy of the fragments in the anisotropic component of the angular distribution suggests that after the impulsive electron-induced bond cleavage the alkyl fragment exits along the C−Br bond direction with very little or no interaction with the surface or neighboring adsorbates. Finally, given the similar dynamics exhibited by the propyl fragments, it is reasonable to believe that the fast channel has a similar origin.

The slow and trapped channels appear to arise from a more complicated process. To better understand the origin of these channels it is instructive to consider their relationship to the overall dissociation process. We begin by characterizing the photodissociation process at 193 nm for all three molecules by looking at the amount of the monolayer removed as photon exposure is increased. The amount of the monolayer lost is, as explained earlier, measured by comparing the integrated molecular desorption signal between the pre- and postirradiation TPD spectra. Since in this case we measure the total molecular loss, each point includes contributions from all three channels.

Figure 8 shows these data (open circles) for methyl bromide ($n = 1$), ethyl bromide ($n = 2$), and propyl bromide ($n = 3$). The solid curve in all three figures is a least-squares fit to the amount of the monolayer dissociated (N_{diss}) with the function:

$$N_{diss} = N_d[1 - \exp(-\sigma_d \gamma)] \quad (4)$$

where N_d and σ_d are adjustable fitting parameters. We have employed this analysis of the data to calculate the total dissociation cross section for the three molecules at 193 nm.[6,9] We found that this cross section for dissociation increases with chain length. A detailed discussion of the chain-length-dependent physics of the cross section for these three systems is presented in ref 6. The data in Figure 8 will be used below to compare the evolution of the slow and trapped channels as a function of photon exposure with that of the total dissociation process.

The dependence of the slow channel with total exposure was measured by recording the integrated TOF signal during exposure at the surface normal since at 0° only the slow component is present in the TOF. For the trapped channel, the total number of alkyl radicals retained on the surface is simply proportional to the area under the postirradiation TPD spectra at the corresponding alkyl mass (see Figure 9). In Figure 8 the

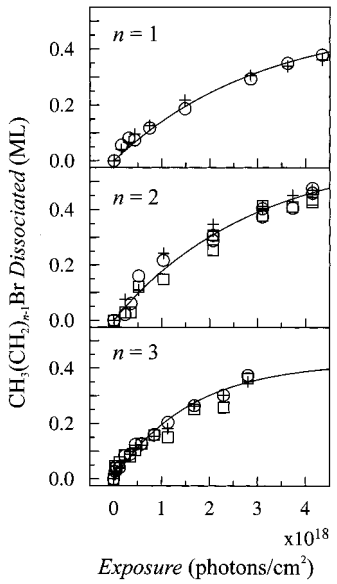

Figure 8. The fraction of a monolayer (open circles) of adsorbed $CH_3(CH_2)_{n-1}Br$ dissociated after exposure to various amounts of 193-nm radiation. Crosses and squares represent the integrated TOF signal at 0° (slow channel) and the trapped alkyl fragments, respectively.

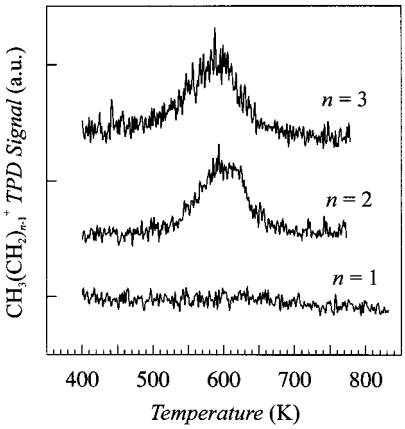

Figure 9. Postirradiation TPD spectra showing desorption of ethyl and propyl species (top two traces). As illustrated by the lower trace, methyl species were not observed to chemisorb.

number of alkyl fragments detected in the slow and trapped channels is plotted with crosses and open squares, respectively. As shown in Figure 9, for methyl bromide no hydrocarbon species were detected in the postirradiation TPD spectra other than the undissociated methyl bromide remaining from the initial monolayer; that is, no detectable evidence of the trapped channel was found. In Figure 8 the data for the slow channel and the trapped channel have been arbitrarily scaled along the *y*-axis. Several experimental unknowns prevent us from quantifying the percentages of the monolayer dissociated that are directed into the three exit channels. For example, with the exception of ethyl radicals, detailed information on the cracking patterns of the different alkyl radicals was not available. The relative sensitivity of the QMS for the three alkyl species was also not known. Furthermore, in the case of the trapped channel, the partial β-hydride elimination of the ethyl and propyl surface-bound species added further uncertainty to the analysis.

Nevertheless, these plots show that the slow and trapped channels scale with the total amount of the monolayer dissociated. Specifically, the two channels "roll over" at the same photon exposure as when the total dissociation process starts to approach its asymptotic limit. We also observe a linear

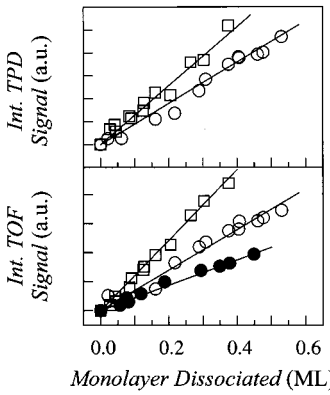

Figure 10. Lower panel shows the integrated TOF at 0° and top panel shows the integrated TPD of the fragments trapped on the surface for methyl (solid circles), ethyl (open circles), and propyl (squares) fragments as a function of the initial monolayer dissociated.

relationship between the total amount dissociated and the amount of alkyl radicals in the slow channel and the trapped channel. Figure 10 shows the integrated TOF signal of the slow channel for methyl (solid circles), ethyl (open circles), and propyl (squares) as a function of the total monolayer dissociated. This figure also shows the corresponding plot for the trapped channel for the larger alkyl bromides. Although the rate of photolysis is decreasing (see Figure 8), as does the adsorbate coverage with increasing photon exposure, the fraction of the total number of fragments that are partitioned into the different energetic channels remains the same. If one of these channels, for example, resulted from molecular dissociation at a minority surface site, then these channels would not be expected to saturate at the same photon exposure.

These results strongly suggest that these two energetically distinct channels have their origins in the same dissociation event and are different dynamical manifestations of a single dissociation process. This implies that the sum of the alkyl fragments from the three channels (i.e., fast, slow and trapped) would equal the total amount of the monolayer dissociated. However, as pointed out above, it was not possible to quantify absolutely the individual contributions of the three channels to the total amount dissociated. We believe that the slow, and trapped fragments are the result of energy loss to the surface after the dissociation event due to the presence of an attractive surface potential. The fragment−surface interactions and their effects on the fragment dynamics are considered in the following section, as are possible origins of the slow-fragment channel.

4. Discussion

In this section, we will present a more detailed discussion of three particularly important observations presented above: the origin of the slower, isotropic fragment distribution, the chain-length dependence of the average energy in the fast, directly ejected fragment distribution, and the chain-length dependence of the fragment angular distributions.

4.1. Origin of the Slow-Fragment Distribution. As shown in Figure 2 the slow channel is more prominent in the angular distributions of the ethyl and propyl fragments than in that of the methyl fragments. Further, while its isotropic angular distribution would suggest directional randomization by scattering, the fragment energies in this channel are comparatively high, having a large fraction of the energy of the directly ejected fragments. In our prior study, multiple explanations were considered for the presence of the slow component in the TOF from an ethyl bromide-covered surface.[5]

For example, the lower energy (compared to the fast channel) of these fragments and the $\cos^m \theta$ angular distribution suggested that these fragments may have undergone inelastic collisions with neighboring adsorbates prior to ejection from the surface. Such collisions would explain the loss of energy and the scrambling of the desorption direction giving rise to an angular distribution that is symmetric about the surface normal. However, this was ruled out as a possible explanation on the basis that the desorption dynamics of ethyl fragments from a GaAs(110) surface covered with only 0.2 and 1 ML were found to be very similar.[5] At the lower coverage, in the absence of any adsorbate islanding,[29] fragment collisions with surface adsorbates would be significantly reduced.

Furthermore, the results from our current study are consistent with the earlier finding that the fragment dynamics are relatively insensitive to surface coverage. The total, accumulated number of fragments in the slow channel for all three adsorbates increases linearly as irradiation of the surface causes the adsorbate to decrease from 1 to ca. 0.4 ML (see Figure 10). If the fragments in the slow channel were merely due to inelastic collisions with neighboring adsorbates, the integrated TOF signal would be expected to deviate from this linear behavior. Additional surface-bound species (Br, trapped alkyl radicals) may affect the fragment dynamics. However, on the basis of the similar dynamics observed (i.e., $\cos^m \theta$ distribution and the above-described linear dependence of the fragment yield with photons) for the slow channel of all three species, in conjunction with our previous conclusions for the ethyl fragment dynamics, we believe that the slow component in the TOF is *not simply* a result of fragment-adsorbate collisions.

The photofragments might also lose energy via collisions with the bare surface after molecular dissociation. In fact, experimental and theoretical studies on photodissociation of methyl halides on insulator surfaces have previously reported this effect and shown that it leads to bimodal velocity distributions. For example, Fairbrother et al.[17] observed two energetically distinct methyl fragments from the direct photolysis of methyl iodide adsorbed on MgO(100). The methyl fragment distributions in their study had peak energies of ∼1.8 and ∼0.01 eV. The low, thermalized energy of the latter distribution was attributed to multiple collisions leading to quasi-equilibration with the surface.[17] Huang et al. modeled the photodissociation of the closely related system, methyl iodide/LiF(100), and reproduced these experimental findings.[30]

In both the experimental and theoretical studies, the two channels were explained as arising from two different initial orientations of the adsorbate where the C−I bond was perpendicular to the surface: (i) methyl pointing toward the vacuum with the iodine toward the surface (gave rise to the fast fragments) and (ii) methyl between the iodine and the surface (gave rise to the slow fragments). In the latter case, the energetic methyl fragment is temporarily trapped between the heavy iodine atom and the underlying surface after the dissociation of the C−I bond. These fragments suffer multiple collisions with the surface and the iodine atom and, therefore, lose much of their initial kinetic energy before finally escaping into the vacuum.

It is very unlikely that the slow channel observed for the alkyl bromide/GaAs(110) system is due to temporary trapping of the alkyl radicals between the surface and the bromine. First, the sum of our investigations of these systems argues strongly against the existence of a significant population of "bromine-up"-oriented molecules. In the case of the insulators, evidence for the alternating molecular dipole orientation is deduced from phase transitions observed in studies of the coverage dependence

of the TPD spectra (e.g., in the case of the methyl iodide/MgO(100) system[18]). This behavior was deduced from the lack of shifts in the desorption-peak temperature with coverage. For the alkyl bromide/GaAs(110) system, a smooth *decrease* in peak temperature with increasing coverage up to a full monolayer is seen, indicating repulsive lateral interactions among similarly oriented dipoles; no evidence of a phase transition due to dipole alignment changes is found.[4−6,20] A similar behavior is observed in the thermal desorption of CH_3Br from Pt(111), where work function measurements have established that molecules adsorb with the Br facing the surface and the C−Br bond nearly parallel to the surface normal.[31] In addition ab initio calculations of methyl bromide on GaAs(110)[15] have demonstrated that the orientation of the methyl bromide on the surface is controlled by strong molecule−substrate interactions. Taken together, these results strongly suggest that, at coverages $\leq$ 1 ML, alkyl bromides on GaAs are oriented such that their dipoles are aligned in the same direction, viz. that with the hydrocarbon end pointing away from the surface.

A second argument against the attribution of slow alkyl fragments to the dissociation of "bromine-up"-oriented molecules on the GaAs(110) surface is based on quantitative consideration of the energetics observed for the slow channel. In our measurements, the slow alkyl fragments have at *least* 50% of the energy of the fast, directly ejected fragments. This is substantially more energy than is found for the methyl fragments rebounding from the LiF or MgO surface, where the energy of slow fragments is ~1% of that of the fast fragments. For the GaAs case, the slow fragments are markedly hyperthermal [$\langle E \rangle = 0.4-1.2$ eV, corresponding to temperatures ($T = \langle E \rangle / 2k_B$) in the range of ~2300−7000 K], whereas for the case of transient trapping observed by Fairbrother et al., the slow methyls are ejected with a velocity distribution characterized by a temperature of only 155 K, close to the surface temperature in those experiments (115 K).[17] On the basis of the consideration of the energetics, as well as the results of the TPD studies discussed above, we conclude, therefore, that no significant population of "bromine-up" molecules exists in monolayers of methyl, ethyl, and propyl bromide on the GaAs(110) surface and, indeed, that the slow channel cannot be attributed to the dissociation of "bromine-up"-oriented molecules.

Bimodal energy channels also have been observed for the photodissociation of methyl bromide on alkali halide surfaces (LiF, NaCl).[32] In this case, the slow component of the distribution was attributed to a collisional displacement of a methyl group from a neighboring methyl bromide molecule by a hot methyl photofragment. Again, in this case molecular orientation plays a key role in this process, which requires that the C−Br bond of the dissociating molecule lie parallel to the surface. For example, on LiF surfaces, methyl halide orientation changes with coverage, going from a parallel to perpendicular alignment as coverage increases; this change caused a concomitant drop in the lower-energy CH_3 channel. The lack of strong coverage dependence[4,5] (up to 1 ML) in our velocity and angular distributions argues for a different origin for the dynamics of our systems. Furthermore, Polanyi and co-workers are careful to point out that although the energies of the slow and fast channels differ by 1−2 eV, the widths of the energy spectra for the departing fragments in the two channels are comparable. This similarity in energetic widths corroborates the concept that the inelastic event is a result of a well-defined single collision between a CH_3 radical and its CH_3Br neighbors. This observation is strongly contrasted by our measurements which reveal that, in our case, the slow alkyl channel is significantly broader than the fast alkyl channel (approximately a factor of 2 times broader in the ethyl bromide case). This suggests that, for the alkyl bromides on GaAs(110), the energy loss responsible for evolution of the slow channel is likely due to multiple collisions and not a well-defined methyl-exchange encounter.

We believe that the results of our current study confirm our earlier interpretation of the ethyl fragment dynamics[5] and suggest that it applies, more generally, to the dynamics of methyl and propyl fragments as well. In this interpretation, photofragmentation of adsorbed alkyl halides, which exist in a distribution of librational states, leads to ejection of alkyl fragments with a range of energies and directions. While a significant fraction of the photofragments initially possess sufficient normal energy to escape the surface (fast channel), other fragments are temporarily trapped by the radical−surface potential energy well and undergo single or multiple collisions with the surface resulting in significant translational energy loss. The initial direction of these scattered fragments is also scrambled, resulting in a more isotropic angular distribution. In addition, during this scattering process, some alkyl fragments encounter surface sites at incident energies and impact and orientation parameters appropriate to the formation of strong chemical bonds thereupon, resulting in the retention of significant quantities of the alkyl radicals on the surface.

Although the details of the potential energy surface (PES) for the alkyl-GaAs(110) system are not known, support for the above-described dynamical model can be gathered from molecular scattering data found in the literature for related systems. For example, Madix and co-workers have developed a molecule−surface potential to model the results of their scattering studies of ethane from Pt(111).[33−36] The depth and range of the alkyl−surface interaction suggest that the radicals created in our system, a few angstroms away from the surface (~3 Å,[15] a typical distance for physisorbed molecules), would be expected to experience significant attractive forces. The methyl−platinum potential used by Madix and co-workers also reproduced their experimental ethane adsorption energy of 0.29−0.33 eV, as measured by TPD. From TPD data we have estimated a desorption energy for ethyl radicals from GaAs(110) at 0.70 eV,[5] making the gas−surface interaction significantly stronger in our case than the ethane−platinum interaction.

There are several contributions to the strong radical−surface interaction. One important contribution is the surface-dipole−molecule interaction; strong permanent dipoles are known to exist on reconstructed GaAs surfaces.[37,38] Another is the chemical interaction between the empty (or filled) dangling bonds at the GaAs(110) surface with electrons (or unoccupied orbitals) of incident species.[39,40] The effect of such forces has been observed in the trapping of trimethylgallium on GaAs surfaces[41] and in the scattering of NH_3 from GaAs(100).[42] In the latter case, the depth of the potential was measured at ~0.5 eV,[42] close to the adsorption energy (~0.35 eV).[43] TOF measurements of the scattering of NH_3 from the GaAs surface revealed two components: a slow component due to long surface residence times—attributed to inelastic scattering resulting in significant translational energy loss—and a faster component due to direct scattering. These channels are analogous to our slow and fast components, and given the similarities between our system and the NH_3/GaAs(100) system, we expect that the slow-alkyl-fragment channel can be attributed to a similar inelastic scattering mechanism.

4.2. Chain-Length Dependence of the Kinetic Energy of the Directly Ejected (Fast) Alkyl Fragments. In this section

we will discuss the chain-length dependence of the average kinetic energy of the directly ejected fragments (see in Figures 3 and 4). In the section which follows we will consider how the observed decrease in the fragment average kinetic energy with increasing chain length is responsible for changes in the angular distributions of the alkyl photofragments.

Increasing the chain length of alkyl fragments increases the mass of the desorbing species as well as the number of internal degrees of freedom; both can effect the kinetic energy of the alkyl radical. Consider, first, the mass effect. Because of the relatively heavy mass of the parent molecule, the increase in fragment mass from methyl to propyl bromide would be expected to cause a relatively small decrease in fragment energy. (We neglect here the increase in the effective mass of the parent molecule due to the (weak) interaction with the GaAs substrate, which would tend to lessen the mass effect.) Specifically, studies have shown that dissociative electron attachment to the normal halocarbons can be described by treating the molecules as quasidiatomics, RX, with R = C_nH_{2n+1} and X = Cl, Br, I.[7] Within this assumption, using conservation of energy and momentum, the maximum kinetic energy, E_n^{kin}, of the alkyl fragment can be expressed as:

$$E_n^{kin} = (1 - \beta_n)E_{avail} \tag{5}$$

where E_{avail} is the energy available after R−Br bond dissociation and β_n is the ratio of the alkyl fragment mass to the parent molecule mass. In the absence of any energy loss during the desorption process or internal excitation of the fragments, E_n^{kin} should be the kinetic energy measured in the *fast channel* (see Figure 4). Given the relevant potential energy curves for these three molecules, it should be possible to estimate E_{avail}. Unfortunately, the exact nature of the potential energy curves for these molecules in proximity to the crystal surface is not known. Nevertheless, it is known that the gas-phase ground-state and excited-state anion potential energy curves for ethyl and propyl bromide are very similar (in contrast to those for methyl bromide)[6,44,45] and that perturbations introduced by proximity to the surface are expected to be similar for these two molecules.[6] Thus, it is reasonable to assume that E_{avail} is approximately the same for the ethyl and propyl fragments. Equation 5 can then be used to scale the kinetic energy shift between propyl and ethyl fragments. Using the average energy of the ethyl fragment fast channel (∼1.1 eV, see Figure 4) for E_2^{kin} to estimate the value of E_{avail} from our measurements at 193 nm, based purely on mass considerations, eq 5 predicts an average energy of 0.9 eV for the propyl fragments. The measured value of 0.7 eV is significantly less than the predicted value, suggesting that simple momentum considerations cannot completely account for the observed trend with chain length.

One reasonable explanation for the observed strong reduction in translational energy with increasing chain length is increased energy partitioning into internal degrees of freedom of the fragment. Several previous studies of the dissociation of alkyl halides via direct photolysis in the gas phase have shown that excitation of internal rovibrational modes increases with chain length. For example, results from the photodissociation of a series of alkyl iodides at 248 nm[46] and alkyl chlorides at 193 nm[47] showed that the amount of the energy that is imparted to the alkyl fragment which is actually partitioned into the translational energy of the fragment is reduced from ∼90% to ∼50% when the hydrocarbon moiety is changed from methyl to *n*-propyl. A similar change would be expected for dissociative electron attachment, since in both cases population of the σ^* orbital leads to a strongly impulsive force along the C−X bond axis.[48] In this regard, it is interesting to compare the partitioning into translational energy by comparing the average kinetic energies, $\langle E\rangle_n$, of the fragments, as a function of chain length. We consider the ratio:

$$I_n = \frac{\langle E\rangle_n}{\langle E\rangle_1} \tag{6}$$

for methyl, ethyl, and propyl fragments produced in three cases: photodissociation of gas-phase alkyl chlorides and iodides and dissociative electron attachment of bromides adsorbed on GaAs(110). Using kinetic energies obtained from refs 46 and 47, as well as those measured for the fast-channel alkyl fragments, we plot I_n as a function of the number of carbons in the molecule in the inset in Figure 4. As shown in the inset, for the gas-phase iodides (white bars) and chlorides (black bars), I_n is observed to decrease monotonically with increasing chain length. In addition, comparison of the chloride to the iodide data reveals that this ratio of the translational energies of the ethyl and propyl fragments to that of the corresponding methyl fragments, I_n, is, roughly speaking, independent of the mass of the halide. Plotting the results from our TOF measurements in the same way (hatched bars), we find that the energetics of the ejected alkyl radicals in the case of dissociative electron attachment on the GaAs surface follow a very similar trend. The similarity of our results with those of the gas-phase studies is consistent with increasing energy partitioning into internal degrees of freedom with increasing mass of the desorbing fragment contributing to the observed decrease in the average kinetic energy with increasing chain length.

4.3. Effects of Fragment Energy on the Angular Distributions. The differences in the angular distributions discussed in the Results section and illustrated in Figures 2 and 5 and Table 1 indicate that the fragment dynamics are sensitive to the wavelength of the dissociating light and the chain length of the fragment. The data show that an increase in either the wavelength of the dissociating light or the length of the hydrocarbon chain reduces the average energy of the ejected fragments. As discussed above, the observed variations in fragment dynamics suggest that the initial kinetic energy of the fragment determines the extent to which its trajectory is affected by the surface-potential well and whether it will desorb or become trapped on the surface. In this section, we consider the relation between kinetic energy and the fragment dynamics in further detail.

As mentioned above, the three alkyl halides studied here undergo substrate-mediated dissociation. Specifically, hot electrons generated by absorption of photons near the surface generate a distribution of energetic electrons that can attach themselves to the adsorbate, initiating C−Br bond cleavage. From conservation of energy, it follows that the energy available for fragment translation depends on the initial energy of the attaching electron, which in turn varies with the wavelength of the incident light. As the photon wavelength is increased from 193 to 351 nm, the average energy of the impinging electrons decreases. As a result, the average energy of the fragments produced via dissociative attachment will also decrease with increasing wavelength. Qualitatively, as shown in Figure 5, we have observed such a decrease for all three molecules; however, the actual change in the fragment energy is certainly not as large as the change in the incident photon energy. The reason for this difference most probably lies in the details of the relative positions of the ground-state molecule and excited-state anion PES and competing processes such as reneutraliza-

tion due to quenching, as well as the exact nature of the fragment−surface PES.

Consider now the implications that the observed correlation between photon energy and fragment energy has on the dynamics of the fragments. The effect of increasing wavelength on fragment dynamics is clearly seen in Figure 5, which shows that a decrease in the average kinetic energy of the fragments is accompanied by an increase in the percentage of slow-channel fragments, as expressed in the ratio *R*. This variation is consistent with the dynamics of less energetic fragments being more strongly modified by the surface potential. The most striking aspect of the data in Figure 5 is that for fragment energies less than ∼0.7 eV: the proportion of slower, scattered fragments increases significantly. Thus, fragments with average kinetic energy above 0.7 eV, viz., methyl fragments at all three wavelengths and ethyl fragments at the two shorter wavelengths, have a large direct/scattered signal intensity ratio. However, fragments with kinetic energies below ∼0.7 eV, viz., the ethyl fragments at 351 nm and the propyl fragments at all three wavelengths, have a lower direct/scattered intensity ratio, and this ratio decreases rapidly with decreasing fragment energy. This correlation of fragment kinetic energy with changes in the anisotropy of the fragment angular distribution strongly suggests the presence of a characteristic energetic threshold of ∼0.7 eV. Fragments that have an energy below this value lose a larger fraction of their original energy, spend more time in the near-surface region, and lose "memory" of their initial adsorption orientation.

Recall that the average energy of the slow channel for propyl fragments at all wavelengths and that for ethyl fragments at 351 nm is ∼0.4 eV (see Figure 6). Taking a simplistic view, one might expect that the average energy of the fragments in the slow channel as a function of decreasing wavelength would increase in a manner similar to the $\langle E \rangle$ shown in Figure 5. It is not clear why the slow fragments for these cases all have the same average energy and why this average energy is less than the ∼0.65 eV observed for the ethyl fragment slow channel at 248 and 193 nm. However, it is interesting to note that for the cases where the average energy of the slow channel is ∼0.4 eV, the total $\langle E \rangle$ of the fragments is below the energetic threshold for desorption (see Figure 5): the final average energy of the slow channel for fragments created with an $\langle E \rangle$ below the energetic threshold has a value that is less than that for fragments created above the threshold. We believe this effect to be the result of greater energy loss to the surface due to prolonged interaction between the fragment and the surface.

Given the arguments above, we should expect the number of fragments trapped on the surface to increase as the initial energy of the fragments is reduced. The lower the average energy of the fragment, the less likely it is to escape the attractive part of the fragment−surface potential. We can examine the effects of the attractive surface potential on the trapping of fragments with decreasing average kinetic energy by quantifying the amount of trapped alkyl fragments as a function of wavelength. Figure 11 shows the area calculated from the postirradiation TPD spectra of trapped propyl fragments as a function of photon energy. The TPD area has been normalized for the total amount of the monolayer dissociated to account for the different cross sections at the three wavelengths.[6] The figure shows an increase in the trapping of propyl fragments as the incident photon energy is reduced from 6.4 to 3.5 eV. We believe that the increase in the amount of propyl fragments retained on the surface with decreasing photon energy is direct evidence of a correlation between the enhancement in fragment trapping with a decrease in fragment energy.

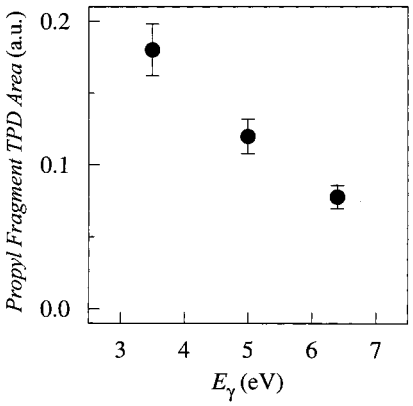

Figure 11. Number of propyl fragments accommodated on the surface for the three photon energies, E_γ.

Furthermore, the absence of a trapping channel for the methyl fragments is consistent with these arguments. In terms of the energetics, a decrease in the chain length of the fragments results in an increase in the average energy of the desorbing species (see Figure 4). Therefore, we do not observe a trapping channel for the methyl fragments, which have significantly higher average kinetic energies than the ethyl and propyl fragments. Similarly, we expect that the number of propyl fragments retained on the surface should exceed the number of ethyl fragments. Unfortunately, as discussed in the Results section, because of various experimental unknowns, we were unable to make absolute measurements of the fraction of the fragments retained on the surface following dissociation and so are unable to make direct comparisons between the ethyl and propyl systems.

However, a careful interpretation of the angular distributions in Figure 2 can provide an indirect evaluation of the amount of partitioning of the fragments into the slow and trapped channels with increasing chain length. For example, from the discussion above, it is reasonable that the angular distribution for $n = 2$ has a significantly greater isotropic component than that for $n = 1$ because of the lower average energy of the ethyl fragments. Likewise, we might expect that the fraction of the slow channel in the propyl angular distribution would be significantly more pronounced than for either of the two shorter-chained fragments. In fact, however, the data in Figure 2 shows that this is not the case; the slow component has a smaller contribution to the total angular distribution for the propyl fragments than that for the ethyl fragments. We believe this observation is explained by the possibility that a greater fraction of the scattered propyl fragments were trapped on the surface, resulting in a drop in the relative importance of the slow-component feature.

The presence of an attractive potential well has been known to affect the angular distribution of desorbing fragments.[49,50] For example, Clinton[51] and Miskovic et al.[49] have shown that the trajectories of desorbing ions in electron-stimulated desorption ion angular distribution (ESDIAD) measurements can be distorted by the image potential and that it is possible for the desorbing species to be captured by the surface when the initial kinetic energy is insufficient to overcome the attraction of the potential. Although the range of the image−charge interactions responsible for these effects is certainly longer than in the case of the alkyl−surface potential, similar deflection and trapping of fragments may be expected to occur. The alkyl−surface potential is not expected to vary by much across chain length due to the similar desorption temperatures of propyl and ethyl radicals during TPD measurements. Therefore, compared to the ethyl fragments, propyl fragment trajectories ending in surface

accommodation become more significant because the average kinetic energy is considerably smaller (at 193 nm by more than 30%), while the fragment−surface potential has not changed significantly.

In addition, the trend for the alkyl radicals appears to parallel the trend in trapping probability that has been observed in the molecular-beam scattering of alkanes from Pt surfaces.[33−36] In these experiments, an increase in the chain length (methane, ethane, propane) resulted in an enhancement of the sticking probability of the alkane on Pt(110)[35] and Pt(111).[36] For example, at normal incidence, with an energy of 0.21 eV, the sticking probability on Pt(111) for methane, ethane, and propane is 0.15, 0.6, and 0.8, respectively. The increases in the molecular weight and the molecular complexity of the scattering species were believed to be responsible for the observed enhancement of the sticking probability. The additional degrees of freedom available to the propane molecules act to enhance the dissipation of translational energy and favor trapping on the surface. It is reasonable to conclude that these same factors would cause an increase in the trapping channel for the longer-chained alkyl radicals. Furthermore, fragments desorbing at larger angles from the surface normal will be preferentially trapped because their smaller perpendicular momentum (compared to that of fragments desorbing close to the surface normal) will decrease their probability of overcoming the surface attraction.[5,49,51] Overall, trapping, in general, and *preferential* trapping of fragments scattered at large angles are expected to increase with a decrease in the kinetic energy and an increase in the number of degrees of freedom of the fragments. Thus we might expect the measured angular distributions to show a less pronounced (on an absolute scale) and sharper slow component for $n = 3$ than for $n = 2$. This latter expectation is in agreement with our measurements (see Table 1) where the width of the slow channel is found to go as $\Delta W_s^1 \approx \Delta W_s^2 > \Delta W_s^3$.

5. Conclusions

Our results have shown the interrelation between fragment kinetic energy and fragment dynamics following the impulsive event resulting from substrate electron attachment to a series of short-chain alkyl bromide molecules. The most energetic fragments were found to be ejected preferentially in a relatively narrow angular distribution centered at ∼30−40° from the surface normal in the plane defined by the normal and the [01] direction. The angular distributions and high kinetic energies of the methyl, ethyl, and propyl fragments are indicative of direct ejection (without scattering), indicating that for all three molecules the adsorbates are preferentially oriented on the surface with their molecular axes canted at ∼30−40° from the surface normal and the bromine ends of the molecules facing the surface. Fragment energies were observed to decrease due to two factors: (i) increasing fragment mass and (ii) decreasing photon energy. In either case, with decreasing kinetic energy, the fragments showed an increased tendency to undergo surface scattering. Scattering trajectories were observed to divide into two regimes: (i) those involving one to several collisions with the surface, enough to randomize the initial trajectory and result in a decreased but still significantly hyperthermal fragment kinetic energy, and (ii) those resulting in complete accommodation with the surface and, hence, adsorption.

Our measurement of a strong decrease in fragment kinetic energy with increasing chain length suggests that the dynamics is heavily influenced by the partitioning of the impulsive energy of the dissociation event into internal degrees of freedom of the alkyl radicals. Such partitioning would most directly be detected by spectroscopic measurement of the internal states of the alkyl radicals. Such a measurement of the internal energies of the methyl radicals using resonantly enhanced multiphoton ionization (REMPI) detection is certainly feasible,[17] and determination of the rotational and vibrational temperatures of the direct and scattered fragments would provide further insight into the dynamics in this case. Such a thorough determination of the internal energy content of the dissociation products in the case of the longer-chain homologues is more difficult and will likely require application of a higher-resolution technique, such as IR laser spectroscopy.[52]

In addition, it has become increasingly clear that gaining a detailed understanding of the microscopic origins of dynamical effects such as those reported here will involve increasingly sophisticated computer simulations.[30,53,54] With the aid of computer models, experimental molecular dynamics measurements, such as those reported herein, hold great promise for providing quantitative insights into the gas−surface interaction potentials which govern these complicated chemical systems.

Acknowledgment. We gratefully acknowledge support of this work by DOE (Contract DEFG02 90ER14104) and NSF (Contract DMR 96-32456).

References and Notes

(1) Marsh, E. P.; Tabares, F. L.; Schneider, M. R.; Gilton, T. L.; Meir, W.; Cowin, J. P. *Phys. Rev. Lett.* **1988**, *60*, 2551.
(2) Zhou, X. L.; Zhu, X. Y.; White, J. M. *Surf. Sci. Rep.* **1991**, *13*, 76.
(3) Ukrainstev, V. A.; Long, T. J.; Harrison, I. *J. Chem. Phys.* **1992**, *96*, 3957.
(4) Lu, P. H.; Lasky, P. J.; Yang, Q. Y.; Osgood, R. M., Jr. *Chem. Phys.* **1996**, *205*, 143.
(5) Khan, K. A.; Moryl, J. E.; Slater, D. A.; Lasky P. J.; Osgood, R. M., Jr. *J. Phys. Chem. B* **1997**, *101*, 9077.
(6) Khan, K. A.; Camillone, N., III; Osgood, R. M., Jr. *J. Chem. Phys.* **1999**, *110*, 10526.
(7) Rowntree, P.; Sanche, L.; Parenteau, L.; Meinke, M.; Weik, F.; Illenberger, E. *J. Chem. Phys.* **1994**, *101*, 4248.
(8) Ayotte, P.; Gamache, J.; Bass, A. D.; Fabrikant, I. I.; Sanche, L. *J. Chem. Phys.* **1997**, *106*, 749. Sanche, L.; Bass, A. D.; Ayotte, P.; Fabrikant, I. I. *Phys. Rev. Lett.* **1995**, *75*, 3568.
(9) Camillone, N., III; Khan, K. A.; Lasky, P. J.; Wu, L.; Moryl, J. E.; Osgood, R. M., Jr. *J. Chem. Phys.* **1998**, *109*, 8045.
(10) Avouris, P.; Persson, B. N. J. *J. Phys. Chem.* **1984**, *88*, 837.
(11) Dixon-Warren, St. J.; Jensen, E. T.; Polanyi, J. C. *J. Chem. Phys.* **1993**, *98*, 5938.
(12) Yang, Q. Y.; Schwarz, W. N.; Osgood, R. M., Jr. *J. Chem. Phys.* **1993**, *98*, 10085.
(13) Yang, Q. Y.; Osgood, R. M., Jr. *J. Phys. Chem.* **1993**, *97*, 8855.
(14) Yang, Q. Y.; Schwarz, W. N.; Lasky, P. J.; Hood, S. C.; Loo, N. L.; Osgood, R. M., Jr. *Phys. Rev. Lett.* **1994**, *72*, 3068.
(15) Black, S.; Friesner, R.; Lu, P. H.; Osgood, R. M., Jr. *Surf. Sci.* **1997**, *382*, 154.
(16) Lasky, P. J.; Lu, P. H.; Yang, M. X.; Osgood, Jr., R. M.; Bent, B. E.; Stevens, P. A. *Surf. Sci.* **1995**, *336*, 140.
(17) Fairbrother, D. H.; Briggman, K. A.; Stair, P. C.; Weitz, E. *J. Chem. Phys.* **1995**, *102*, 7267.
(18) Holbert, V. P.; Garrett, S. J.; Bruns, J. C.; Stair, P. C.; Weitz, E. *Surf. Sci.* **1994**, *314*, 107.
(19) Dixon-Warren, St. J.; Heyd, D. V.; Jensen, E. T.; Polanyi, J. C. *J. Chem. Phys.* **1993**, *98*, 5954.
(20) Lu, P. H.; Lasky, P. J.; Yang, Q. Y.; Wang, Y.; Osgood, R. M., Jr. *J. Chem. Phys.* **1994**, *101*, 10145.
(21) Meyer, R. J.; Duke, C. B.; Paton, A.; Kahn, A.; So, E.; Yeh, J. L.; Mark, P. *Phys. Rev. B* **1979**, *19*, 10.
(22) Pedrotti, F. L.; Pedrotti, L. S. *Introduction to Optics*, 2nd ed.; Prentice Hall: Englewood Cliffs, NJ, 1993; Chapter 20.
(23) *Properties of Gallium Arsenide*, 3rd ed.; Brozel, M. R., Stillman, G. E., Eds.; INSPEC: London, 1996.
(24) Redhead, P. A. *Vacuum* **1962**, *12*, 203.
(25) Due to a recalibration of our TOF apparatus, the average energies for the ethyl fragments are different from those reported earlier in ref 5.
(26) Yang, Q. Y.; Schwarz, W. N.; Hood, S. C.; Loo, N. L.; Osgood, R. M., Jr. *Surf. Sci.* **1993**, *298*, 195.
(27) Zhu, X.-Y. *Annu. Rev. Phys. Chem.* **1994**, *45*, 113.

(28) Gadzuk, J. W.; Richter, L. J.; Buntin, S. A.; King, D. S.; Cavanagh, R. R. *Surf. Sci.* **1990**, *235*, 317.
(29) Shifts observed in the first monolayer desorption feature in TPD spectra for monolayer and submonolayer coverages are consistent with repulsive lateral interactions, indicating that adsorbate islands do not nucleate during the growth of CH_3Br on GaAs(110).
(30) Huang, Z.-H.; Guo, H. *J. Chem. Phys.* **1993**, *98*, 3395.
(31) French, C.; Harrison, I. *Surf. Sci.* **1997**, *387*, 11.
(32) Garrett, S. J.; Heyd, D. V.; Polanyi, J. C. *J. Chem. Phys.* **1997**, *106*, 7834.
(33) Stinnett, J. A.; Madix, R. J.; Tully, J. C. *J. Chem. Phys.* **1996**, *104*, 3134.
(34) Stinnett, J. A.; Weaver, J. F.; Madix, R. J. *Surf. Sci.* **1998**, *395*, 148.
(35) McMaster, M. C.; Schroeder, S. L. M.; Madix, R. J. *Surf. Sci.* **1993**, *297*, 253.
(36) McMaster, M. C.; Arumainayagam, C. R.; Madix, R. J. *Chem. Phys.* **1993**, *177*, 461.
(37) Pianetta, P.; Lindau, I.; Garner, C. M.; Spicer, W. E. *Phys. Rev. B* **1978**, *18*, 2792.
(38) Northrup, J. E.; Foyen, S. *Mater. Sci. Eng. B* **1995**, *30*, 81.
(39) Mokwa, W.; Kohl, D.; Heiland, G. *Surf. Sci.* **1984**, *139*, 98.
(40) Büchel, M.; Lüth, H. *Surf. Sci.* **1979**, *87*, 285.
(41) Sasaki, M.; Yoshida, S. *Surf. Sci.* **1996**, *356*, 233−246.
(42) Sugawara, S.; Sasaki, M.; Yamamoto, S. *Appl. Surf. Sci.* **1998**, *130*−*132*, 387.
(43) Zhu, X.-Y. *J. Chem. Phys.* **1993**, *98*, 3410.
(44) Wentworth, W. E.; George, R.; Keith, H. *J. Chem. Phys.* **1969**, *51*, 1791.
(45) Modelli, A.; Scagnolari, F.; Destefano, G.; Jones, D.; Guerra, M. *J. Chem. Phys.* **1992**, *96*, 2061.
(46) Zhu, Q.; Cao, J. R.; Wen, Y.; Zhang, J.; Zhong, X.; Huang, Y.; Fang, W.; Wu, X. *Chem. Phys. Lett.* **1988**, *144*, 486.
(47) Kawasaki, M.; Kasatani, K.; Sato, H.; Shinohara, H.; Nishi, N. *Chem. Phys.* **1984**, *88*, 135.
(48) This similarity between these two dissociative events has been noted previously, viz., in harpooning reactions of alkyl halides with alkali metal atoms in crossed molecular beams: Herschbach, D. R. *Adv. Chem. Phys.* **1966**, *10*, 319.
(49) Miskovic, Z.; Vukanic, J.; Madey, T. E. *Surf. Sci.* **1984**, *141*, 285.
(50) Guest, R. J.; Goldby, I. M.; Palmer, R. E.; Bly, D. N.; Hartley, D. M.; Rous, P. J. *Faraday Discuss.* **1993**, *96*, 117.
(51) Clinton, W. L. *Surf. Sci.* **1981**, *112*, L791.
(52) Francisco, T. W.; Camillone, N., III; Miller, R. E. *Phys. Rev. Lett.* **1996**, *77*, 1402.
(53) Watson, J. M.; NoorBatcha, I.; Lucchese, R. R. *J. Chem. Phys.* **1992**, *96*, 7771.
(54) Guo, H.; Liu, L. *Surf. Sci.* **1997**, *372*, 337.